

OPTIMAL DESIGN FOR HIGH-TEMPERATURE BROADBAND RADOME WALL WITH SYMMETRICAL GRADED POROUS STRUCTURE

L. C. Zhou, Y. M. Pei^{*}, R. B. Zhang, and D. N. Fang

State Key Lab for Turbulence and Complex Systems, College of Engineering, Peking University, Beijing 100871, China

Abstract—This study focuses on electromagnetic and thermo-mechanical optimal design for high-temperature broadband radome wall with symmetrical graded porous structure. The position-dependent porosity increases from the two surfaces of the structure to its intermediate layer. Electromagnetic and thermo-mechanical properties of the proposed structure are investigated simultaneously via numerical simulations. Optimal results suggest that the symmetrical porous structure possesses better broadband transmission performance in the 1–100 GHz frequency range, in contrast to a traditional A-sandwich structure. The thermo-mechanical investigation also indicates that the novel structure meets the requirement for high-temperature (up to 1400°C) applications.

1. INTRODUCTION

A radome [1–5] is applied to protection of the delicate antennas mounted on diverse aircraft, such as airplanes or missiles, from severe environments. Those radomes used on supersonic or hypersonic aircraft, may encounter high levels of mechanical and thermal loadings [6]. For example, the radome has to withstand a high temperature of more than 1400°C, if the aircraft is flying at a velocity of more than 5 Mach [7]. More predominantly, the radome must not interfere with the utility of the antenna, which is responsible for communication, detection or imaging [8–11]. Thus, the material that makes up the radome is required to possess relatively low dielectric constant, low dielectric loss, excellent mechanical and thermal properties. A material with better mechanical and thermal

Received 2 March 2012, Accepted 27 March 2012, Scheduled 5 April 2012

* Corresponding author: Yongmao Pei (peiy@pku.edu.cn).

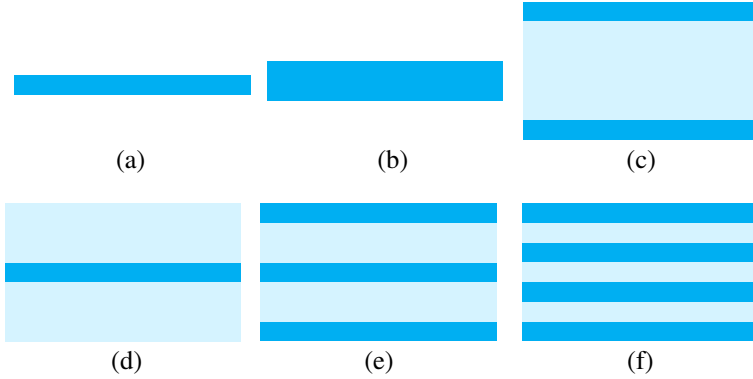


Figure 1. Radome wall structures, (a) thin wall, (b) half-wavelength wall, (c) A-sandwich, (d) B-sandwich, (e) C-sandwich, (f) multilayer.

properties, however, does always exhibit higher dielectric constant. Such contradiction demands optimal design for radome wall structures, especially for high-temperature broadband applications.

Nowadays, radome wall structures, as shown in Fig. 1, involve thin wall, half-wavelength wall, A-sandwich, B-sandwich, C-sandwich and multilayer structures [12–14]. The thin wall structure has relatively low mechanical properties especially for high frequency employments, since its thickness is less than 5% of the operating frequency wavelength. The half-wavelength wall, which is one-half wavelength thick, has a narrow bandwidth of only 5%, and is not suitable for broadband use. Sandwich structures composed of different dielectric layers are commonly applied, due to their broadband properties and high strength-to-weight ratio. For instance, an A-sandwich structure (Fig. 1(c)), which consists of a lightweight and low-permittivity foam core and two dense thin facings, has relatively lower weight but higher strength. This kind of structure has better broadband transmission ability than single-layered structures, and is always employed upon frequencies less than 20 GHz [13].

In high-temperature environments, extreme thermal stress may occur at interfaces of sandwich structures, due to significant temperature gradients and laminations. Sandwich structures are made of several layers with distinct mechanical and thermal properties. Such differences between two bordering layers under high-temperature conditions will result in thermal mismatch stress, which may be the critically vital factor for radome destruction. Since the 1990s, functionally graded materials have been investigated, since their functionally graded designs can efficiently help reduce thermal

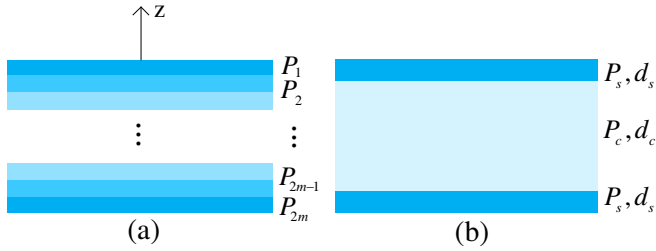


Figure 2. (a) The symmetrical graded porous structure. (b) The A-sandwich structure for comparison.

stress [15–17]. Hence, a symmetrical graded porous structure (Fig. 2(a)) for high-temperature broadband applications is put forward in this paper.

This study carries out investigations on electromagnetic and thermo-mechanical properties of a symmetrical graded porous structure. The transmission efficiency of the proposed structure in the 1–100 GHz frequency range is investigated by the transfer matrix method [18] based on the electromagnetic theory. The thermo-mechanical property of the structure, which is a temperature-dependent problem, is investigated via numerical simulation. Results suggest that the symmetrical graded structure has broadband ability in the 1–100 GHz range, and succeeds in withstanding high-temperature conditions. Its electromagnetic and thermo-mechanical properties are demonstrated to be better than that of the A-sandwich structure for comparison.

2. SYMMETRICAL GRADED POROUS STRUCTURE

In this study, a symmetrical graded porous structure, as shown in Fig. 2(a), is proposed. The position-dependent porosity increases continuously from the outermost and innermost surfaces to the middle of the structure. For simulation simplicity, the proposed structure is assumed to be composed of plenty of layers. Each layer is equal in thickness and has a homogeneous porosity. The porosity distribution is given by the following equation as

$$P_i = P_m \left(\frac{i-1}{m-1} \right)^n \quad (i = 1, 2, \dots, m), \quad (1)$$

where m is one half of the total layer number ($2m$), P_i is the i th layer porosity and n is the graded index that determines how fast or gradually the porosity varies due to position variation. For a

symmetrical structure, one may derive the porosity of each layer to be

$$P_i = P_{2m+1-i} \quad (i = 1, 2, \dots, 2m). \quad (2)$$

From Eqs. (1) and (2), the outermost and innermost layer porosities P_1 and P_{2m} are both evaluated as zero, which means that the outermost and innermost layers are made of fully dense material. In this study, the intermediate layer porosity P_m or P_{m+1} is the maximum porosity, and will be given in Section 3.1. Fig. 3 depicts porosity distributions of the symmetrical graded porous structure as the graded index n varies. It is seen that the porosity decreases simultaneously in each layer when the graded index becomes greater, except for P_1 , P_m , P_{m+1} and P_{2m} , which are given as fixed values. If the graded index tends to zero, each layer excluding the outermost and innermost layers, has a porosity equal to the maximum porosity P_m or P_{m+1} . Thus, the whole structure resembles an A-sandwich structure with a thick foam core and two extremely thin dense skins bounded to the core on its two sides. As the graded index n tends to be infinite, all layers, except for the m th and $(m+1)$ th layers, are fully-densely made. The structure turns to be a sandwich structure with two thick skins and an extremely thin core in this situation.

A traditional A-sandwich structure (Fig. 2(b)) is applied to comparison with the proposed symmetrical graded porous structure (Fig. 2(a)) in this study. It is assumed that the two structures are made of the same material with the same mass. Once the skin and core porosities P_s and P_c , the skin and core thicknesses d_s and d_c of the A-sandwich structure are given, the thickness of each layer Δd in

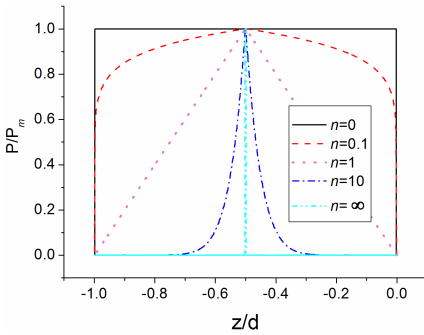


Figure 3. Porosity distributions of the symmetrical porous structure as the graded index n varies.

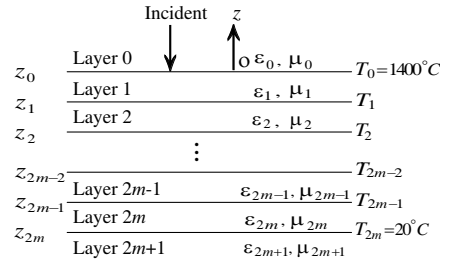


Figure 4. A stratified medium composed of $2m$ dielectric layers, with boundaries at $z = z_0, z_1, \dots, z_{2m}$.

the proposed structure can be derived as

$$\Delta d = \frac{(1 - P_s) \cdot d_s + (1 - P_c) \cdot d_c}{\sum_{i=1}^{2m} (1 - P_i)}. \quad (3)$$

Once the graded index n is given, P_i can be determined by Eqs. (1) and (2). Subsequently, Δd can be evaluated from Eq. (3). And the entire thickness of the symmetrical graded porous structure is obtained as

$$d = 2m \cdot \Delta d. \quad (4)$$

It is seen that the entire thickness d depends on the graded index n , if the mass of the whole structure is given.

3. METHODS

3.1. Transfer Matrix Method

The transfer matrix method (TMM) [18] is used to investigate electromagnetic property of the symmetrical graded porous structure, since it exhibits high efficiency in dealing with transmission and reflection problems of a stratified medium. Consider a plane wave incident upon a stratified medium with boundaries at $z = z_0, z_1, \dots, z_{2m}$, as shown in Fig. 4. It is assumed that the 0th and $(2m + 1)$ th layers are half-infinite, and in this study they are air media. The transfer matrix method displays the relationship between the incident, reflected and transmitted waves as

$$\begin{bmatrix} A_0 \\ B_0 \end{bmatrix} = [V_0][V_1] \dots [V_{2m}] \cdot \begin{bmatrix} A_{2m+1} \\ B_{2m+1} \end{bmatrix} = \begin{bmatrix} V_{11} & V_{12} \\ V_{21} & V_{22} \end{bmatrix} \begin{bmatrix} 0 \\ B_{2m+1} \end{bmatrix}, \quad (5)$$

where $[V_i]$ is the forward propagation matrix, A_0 , B_0 and B_{2m+1} represent the amplitudes of the reflected, incident and transmitted waves respectively. Thus, the transmission efficiency is found to be

$$t_e = 1/|V_{22}|^2. \quad (6)$$

Before using Eq. (6) to estimate the transmission efficiency of the symmetrical graded porous structure, one should first obtain the permittivity of each layer. The permittivity of porous material can be evaluated by Maxwell-Garnett's Formula [19]:

$$\frac{\varepsilon_i}{\varepsilon_1} = 1 + \frac{3P_i}{3\varepsilon_1/(1 - \varepsilon_1) + (1 - P_i)}, \quad (7)$$

where ε_1 is the permittivity of the first layer with fully dense material, and ε_i is the i th layer permittivity. In this study, silicon nitride

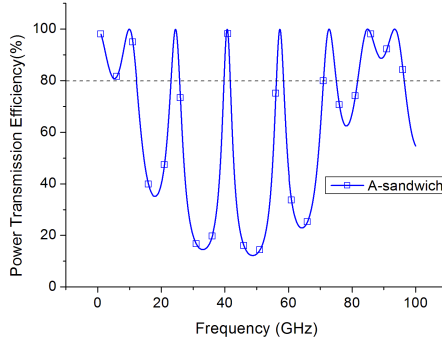


Figure 5. The transmission efficiency of the A-sandwich structure in the 1–100 GHz frequency range.

is chosen as the construction material, for it has excellent thermal and mechanical properties with relatively low permittivity. The permittivity of fully dense silicon nitride is approximately 8.0 [20]. Hence the i th layer permittivity can be estimated by Eq. (7), if P_i is given.

As for the A-sandwich structure for comparison, the thicknesses d_s and d_c , the permittivities ε_s and ε_c are chosen as 0.6 mm, 5.6 mm, 8.0 and 2.0 respectively. The porosities P_s and P_c estimated by Eq. (7) are 0% and 81.0% respectively. Fig. 5 shows the transmission efficiency of the A-sandwich structure in the 1–100 GHz frequency range by TMM. It is seen that the structure is feasible for employments in the 1–12 GHz and 82–96 GHz frequency ranges. In the 12–82 GHz range, however, the structure is limited in its ability to provide sufficient transmission efficiency.

In this study, the outermost and innermost layers of the symmetrical graded porous structure are assumed to be made of fully dense material, namely $P_1 = P_{2m} = 0$. And the maximum porosity P_m or P_{m+1} is assumed to be equal to P_c . Thus, the transmission efficiency of the proposed structure only depends on the graded index n . And we can investigate the effect of the graded index on the transmission efficiency using TMM.

3.2. Method for Steady Temperature Field

The steady temperature field should be obtained in advance before estimation of the steady thermal stress field. As shown in Fig. 4, the temperature at the interface $z = z_i$ is assumed to be T_i , which is a variable to be determined. The boundary conditions for the steady

heat conduction problem are $T_0 = 1400^\circ\text{C}$ and $T_{2m} = 20^\circ\text{C}$. As for the i th layer, the one-dimensional steady heat conduction equation is given as

$$\frac{d}{dz} \left[\lambda(T, P_i) \frac{dT}{dz} \right] = 0, \tag{8}$$

where $\lambda(T, P_i)$ is the temperature-dependent and porosity-dependent thermal conductivity. The thermal conductivity due to porosity variation [21] is given as

$$\lambda(P) = \frac{\lambda_0(1 - P)}{1 + P/2}, \tag{9}$$

and the thermal conductivity due to temperature variation [22] is presented by

$$\lambda_0(T) = \left(43.03 \cdot e^{-T/495.59} + 15.64 \right) \text{W}/(\text{m} \cdot ^\circ\text{C}). \tag{10}$$

By substituting Eq. (10) into Eq. (9), the double-variable-dependent conductivity is obtained as

$$\lambda(T, P) = g(P) \cdot \lambda_0(T), \tag{11}$$

where $g(P) = \frac{1-P}{1+P/2}$ is the porosity factor.

Substituting Eq. (11) into Eq. (8) yields

$$\frac{d}{dz} \left[g(P_i) \cdot \lambda_0(T) \frac{dT}{dz} \right] = 0. \tag{12}$$

The implicit solution for Eq. (12) is found to be

$$g(P_i) \cdot \Psi_{\lambda_0}(T) = M_i z + N_i, \tag{13}$$

where $\Psi_{\lambda_0}(T)$ is a primitive function of $\lambda_0(T)$, M_i and N_i are constants to be determined.

At the boundary $z = z_i$ ($i = 1, 2, \dots, 2m - 1$), one may obtain

$$\lambda(T, P_i) \frac{dT}{dz} \Big|_{z=z_i} = \lambda(T, P_{i+1}) \frac{dT}{dz} \Big|_{z=z_i}. \tag{14}$$

The boundary condition leads to

$$M_1 = M_2 = \dots = M_{2m} = M. \tag{15}$$

For the i th layer, we may obtain the following equations:

$$g(P_i) \cdot \Psi_{\lambda_0}(T_{i-1}) = M \cdot z_{i-1} + N_i \tag{16}$$

and

$$g(P_i) \cdot \Psi_{\lambda_0}(T_i) = M \cdot z_i + N_i. \tag{17}$$

By subtracting Eq. (17) from Eq. (16), one can obtain

$$\Psi_{\lambda_0}(T_{i-1}) - \Psi_{\lambda_0}(T_i) = \frac{(z_{i-1} - z_i)}{g(P_i)} \cdot M. \quad (18)$$

Thus, one may have

$$\sum_{i=1}^{2m} [\Psi_{\lambda_0}(T_{i-1}) - \Psi_{\lambda_0}(T_i)] = \sum_{i=1}^{2m} [(z_{i-1} - z_i)/g(P_i)] \cdot M. \quad (19)$$

Hence, M can be determined as

$$M = \frac{\Psi_{\lambda_0}(T_0) - \Psi_{\lambda_0}(T_{2m})}{\sum_{i=1}^{2m} [(z_{i-1} - z_i)/g(P_i)]}. \quad (20)$$

By substituting Eq. (20) into Eq. (13) and using the boundary conditions, N_i can be determined. Thus, the implicit solutions for the steady temperature field are acquired.

3.3. Method for Stress Field

For thermo-mechanical optimal design, the thermal stress field in the steady temperature field is to be calculated. The strain only depends on z and can be written as

$$\varepsilon(z) = \varepsilon(0) + \kappa \cdot z, \quad (21)$$

where κ is the curvature and $\varepsilon(0)$ is the strain at $z = 0$.

And the thermal stress [23] is found to be

$$\begin{aligned} \sigma(z) &= \frac{E(T, P)}{1 - \nu(T, P)} [\varepsilon(z) - \alpha(T, P) \cdot \Delta T] \\ &= \frac{E(T, P)}{1 - \nu(T, P)} [\varepsilon(0) + \kappa \cdot z - \alpha(T, P) \cdot (T - 20^\circ\text{C})], \end{aligned} \quad (22)$$

where the temperature-dependent and porosity-dependent parameters $E(T, P)$, $\nu(T, P)$ and $\alpha(T, P)$ are the Young's modulus, Poisson's ratio and linear expansion coefficient, respectively. It should be emphasized that the temperature T and the porosity P in Eq. (22) are functions of the coordinate z .

The linear expansion coefficient α , Young's modulus E , Poisson's ratio ν and strength σ_F due to porosity variation [24–26] are as follows:

$$\alpha(P) = \alpha_0, \quad (23)$$

$$E(P) = \frac{E_0(1 - P)}{1 + \frac{(5 + \nu_0)(37 - 8\nu_0)}{8(1 + \nu_0)(23 + 8\nu_0)} \cdot P}, \quad (24)$$

$$\nu(P) = \nu_0, \quad (25)$$

and

$$\sigma_F(P) = \sigma_{F0} \cdot e^{-\beta \cdot P}, \tag{26}$$

where α_0 , E_0 , ν_0 and σ_{F0} are the fully dense material parameters respectively. The parameters due to temperature variation of Si_3N_4 ceramic [21, 27–29] are as follows respectively:

$$\alpha_0(T) = 2.85 \times 10^{-6}/^\circ\text{C}, \tag{27}$$

$$E_0(T) = 320.4 - 0.0151 \cdot (273.15 + T) \cdot e^{-445/(273.15+T)} (\text{GPa}), \tag{28}$$

$$\nu_0(T) = 0.267 \tag{29}$$

and

$$\sigma_{F0}(T) = 1.03 - 8.26/(1505.20 - T) (\text{GPa}). \tag{30}$$

By substituting Eqs. (27) ~ (30) into Eqs. (23) ~ (26), the material parameters as functions of T and P are obtained as follows:

$$\alpha = \alpha_0, \tag{31}$$

$$E(T, P) = \frac{E_0(T)(1 - P)}{1 + \frac{(5+\nu_0)(37-8\nu_0)}{8(1+\nu_0)(23+8\nu_0)} \cdot P}, \tag{32}$$

$$\nu = \nu_0, \tag{33}$$

and

$$\sigma_F(T, P) = \sigma_{F0} \cdot e^{-\beta \cdot P}, \tag{34}$$

where $\beta = 4.24$ [30]. The linear expansion coefficient and Poisson’s ratio obtained are not relevant to neither temperature nor porosity.

For free mechanical boundary conditions, the force and moment equilibrium equations are as follows:

$$\int_{z_{2m}}^{z_0} \sigma(z) dz = 0, \tag{35}$$

and

$$\int_{z_{2m}}^{z_0} \sigma(z) \cdot z dz = 0. \tag{36}$$

We can solve Eqs. (35) and (36) for κ and $\varepsilon(0)$. Thus, the thermal stress field can be given by Eq. (22).

4. RESULTS AND DISCUSSION

In this section, investigations both on electromagnetic and thermal-mechanical performances of the symmetrical graded porous structure

are enforced by computational simulations. Before the procedure of optimal design, the symmetrical graded porous structure is assumed to be composed of 500 layers, namely $m = 250$. In fact, five hundred layers are rather sufficient to simulate a structure with continuously graded porosity distribution, because each layer would be merely 0.02 millimeter thick for a radome wall structure with a conventional thickness of approximately 10 millimeters. As discussed in Section 3, the properties of the proposed structure merely depends on the graded index n , in case that the entire mass is given as a constant value. Thus, the influences of the graded index on the electromagnetic and thermal-mechanical properties are simultaneously studied below.

4.1. Effect of the Graded Index on the Transmission Property

The effect of the graded index n on the transmission property of the symmetrical graded porous structure is shown in Fig. 6. The figure manifests a descending transmission ability of the structure due to an increase in the graded index. As the graded index is barely 0.01, which is considerably close to zero, the transmission efficiency maintains a high lever (greater than 80%) in the whole frequency range. Such superior transmission ability results from the fact that the symmetrical graded porous structure tends to be a foam core with two extremely thin facings, if the grade index approaches zero. As the graded index approaches infinity, the graded structure tends to be composed of fully dense material, because the intermediate porous layer is extremely thin and can be neglected. Such a high-permittivity material apparently results in deficiency of transmission ability. The simulation result also indicates that the symmetrical graded porous structure satisfies broadband transmission requirement in the 1–100 GHz range, if the graded index is less than 0.1. It is seen that the graded structure, with a graded index less than 0.1, exhibits much better broadband transmission property than the A-sandwich structure, which is only feasible in the 1–12 GHz and 82–96 GHz ranges.

4.2. Effect of the Graded Index on the Thermo-mechanical Property

Figure 7 shows the stress ratio distributions when the graded index varies. The stress ratio σ/σ_F , due to temperature gradients and laminations, is required to be greater than -1.0 and less than 1.0 in order to withstand high-temperature conditions [31]. For the A-sandwich structure, we can see that the stress ratio at the boundary of the outer skin layer and the core layer is stepped. The stress ratio σ/σ_F

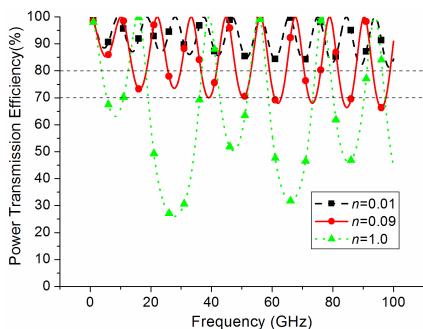


Figure 6. The effect of the graded index n on the transmission efficiency of the symmetrical graded porous structure.

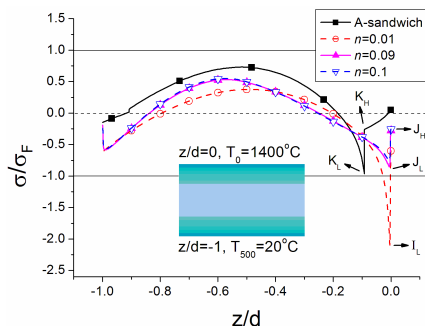


Figure 7. The effect of the graded index n on the thermo-mechanical property of the symmetrical graded porous structure.

at Point K_H in Fig. 7 is merely -0.26 , while it is approximately -1.0 ($\sigma/\sigma_F = -0.96$) at Point K_L . The difference of the stress ratios is on account of different strengths due to porosity variation at Points K_H and K_L . It is seen from Fig. 7 that the stress ratio in the symmetrical graded porous structure becomes as low as -2.3 near the outermost skin (at Point I_L), if the graded index n approaches zero. In fact, the outermost skin material is fully dense, while the intermediate layer consists of foam material with a maximum porosity, if the graded index is equal to zero. The two bordering layers are significantly distinct in thermal and mechanical properties. Furthermore, the strength σ_F near the outermost skin is relatively low due to high temperature, and the temperature gradient is relatively high as well. All these factors result in the high thermal stress ratio near the outermost layer. As the graded index increases, thermal stress is efficiently reduced, resulting from impaired gradients of thermal and mechanical properties. Fig. 7 also indicates that the symmetrical graded structure is feasible for high-temperature (up to 1400°C) employments, if the graded index n is in the vicinity of 0.09 . It is seen that the thermal stress of the graded structure is reduced in contrast to the A-sandwich structure, especially at the interface between the outermost skin and its bordering layer, where the stress ratio is at a considerably dangerous value (-0.96 at Point K_L) for the A-sandwich structure and a relatively safe value (-0.85 at Point J_L) for the proposed structure. If a safe factor of about 1.05 is considered [31], the A-sandwich structure would fail to fulfill the requirement of high-temperature conditions. According to the discussion above, we come to a conclusion that the symmetrical graded

structure is feasible for high-temperature broadband applications, if its graded index is about 0.09. And its electromagnetic and thermo-mechanical abilities precede that of the A-sandwich structure for comparison.

5. CONCLUSION

This study focuses on both electromagnetic and thermo-mechanical optimal design for high-temperature broadband radome wall with symmetrical graded porous structure. Optimal results suggest that the symmetrical graded porous structure possesses the best abilities if the porosity graded index is chosen as approximately 0.09. The symmetrical graded structure is demonstrated to be better than the A-sandwich structure in the broadband transmission ability. And the thermo-mechanical investigation also indicates that the novel structure meets the requirement for high-temperature (up to 1400°C) applications.

ACKNOWLEDGMENT

This work was supported by National Natural Science Foundation of China (Grant No. 91016021, 90816019), National Basic Research Program of China (973 Program, 2010CB8327001, 2011CB610303), and Foundation of the Author of National Excellent Doctoral Dissertation of China (No. 201029).

REFERENCES

1. Kozakoff, D. J., *Analysis of Radome Enclosed Antennas*, Artech House, Norwood, MA, 1997.
2. Persson, K., M. Gustafsson, and G. Kristensson, "Reconstruction and visualization of equivalent currents on a radome using an integral representation formulation," *Progress In Electromagnetics Research B*, Vol. 20, 65–90, 2010.
3. Sukharevsky, O. I. and V. A. Vasilets, "Scattering of reflector antenna with conic dielectric radome," *Progress In Electromagnetics Research B*, Vol. 4, 159–169, 2008.
4. Meng, H. F. and W.-B. Dou, "Fast analysis of electrically large radome in millimeter wave band with fast multipole acceleration," *Progress In Electromagnetics Research*, Vol. 120, 371–385, 2011.

5. Xiao, K., S. L. Chai, and L.-W. Li, "Comparisons of coupled VSIE and non-coupled VSIE formulations," *Journal of Electromagnetic Waves and Applications*, Vol. 25, No. 10, 1341–1351, 2011.
6. Amin, A. M. and R. L. Sierakowski, "Effect of thermomechanical coupling on the response of elastic solids," *AIAA Journal*, Vol. 28, No. 7, 1319–1322, 1990.
7. Chen, F., Q. Shen, and L. Zhang, "Electromagnetic optimal design and preparation of broadband ceramic radome material with graded porous structure," *Progress In Electromagnetics Research*, Vol. 105, 445–461, 2010.
8. Karim, M. N. A., M. K. A. Rahim, H. A. Majid, O. B. Ayop, M. Abu, and F. Zubir, "Log periodic fractal Koch antenna for UHF band applications," *Progress In Electromagnetics Research*, Vol. 100, 201–218, 2010.
9. Xu, H.-Y., H. Zhang, K. Lu, and X.-F. Zeng, "A holly-leaf-shaped monopole antenna with low RCS for UWB application," *Progress In Electromagnetics Research*, Vol. 117, 35–50, 2011.
10. Hong, T., M.-Z. Song, and Y. Liu, "RF directional modulation technique using a switched antenna array for communication and direction-finding applications," *Progress In Electromagnetics Research*, Vol. 120, 195–213, 2011.
11. Zhu, F., S.-C. Gao, A. T. S. Ho, T. W. C. Brown, J. Li, and J.-D. Xu, "Low-profile directional ultra-wideband antenna for see-through-wall imaging applications," *Progress In Electromagnetics Research*, Vol. 121, 121–139, 2011.
12. Koetje, E. L., F. H. Simpson, and J. F. Schorsch, "Broadband and high temperature radome apparatus," US Pat., 4677443, Jun. 30, 1987.
13. Mackenzie, S. B., "Radome wall design having broadband and mm-wave characteristics," US Pat., 5408244, Apr. 18, 1995.
14. Mackenzie, S. B. and D. W. Stressing, "W-band and X-band radome wall," US Pat., 6028565, Feb. 22, 2000.
15. Niino, M. and S. Maeda, "Recent development status of functionally gradient materials," *ISIJ International*, Vol. 30, No. 9, 699–703, 1990.
16. Javaheri, R. and M. R. Eslami, "Thermal buckling of functionally graded plates," *AIAA Journal*, Vol. 40, No. 1, 162–169, 2002.
17. Vel, S. S. and R. C. Batra, "Exact solution for thermoelastic deformations of functionally graded thick rectangular plates," *AIAA Journal*, Vol. 40, No. 7, 1421–1433, 2002.
18. Kong, J. A., *Electromagnetic Wave Theory*, John Wiley & Sons,

- Inc., New York, 1986.
19. Garnett, J. C. M., "Colors in metal glasses and in metallic films," *Philosophical Transactions of the Royal Society of London, Series A, Mathematical, Physical & Engineering Sciences*, Vol. 203, No. 359–371, Royal Society, London, 1904.
 20. Huang, X., F. Peng, F. Yan, and H. Tang, "Research on the dielectric properties of composite made with Si_3N_4 - SiO_2 ," *Journal of Wuhan University of Technology*, Vol. 28, No. 12, 21–23, 2006.
 21. Zhou, Y., *Science of Ceramic Material*, Harbin Institute of Technology Press, Harbin, China, 1995.
 22. Kuriyama, M., Y. Inomata, T. Kujima, and Y. Hasegawa, "Thermal conductivity of hot-pressed Si_3N_4 by the laser flash method," *American Ceramic Society Bulletin*, Vol. 57, No. 12, 1119–1122, 1978.
 23. Miao, X., X. Zhang, B. Wan, J. Han, and S. Du, "Research on thermoelastic problems computation methods of FGM," *Journal of Functional Materials*, Vol. 30, No. 2, 122–125, 1999.
 24. Kingery, W. D., H. H. Bowen, and D. R. Uhlmann, *Introduction to Ceramics*, 2nd edition, Wiley, New York, 1976.
 25. Kondo, R., *Porous Materials*, Gihodo, Tokyo, Japan, 1973.
 26. Coble, R. L. and W. D. Kingery, "Effect of porosity on physical properties of sintered alumina," *Journal of the American Ceramic Society*, Vol. 39, No. 11, 377–385, 1956.
 27. Huseby, I. C., G. A. Slack, and R. H. Arendt, "Thermal expansion of CdAl_2O_4 , β - Si_3N_4 and other phenacite-type compounds," *Bulletin of the American Ceramic Society*, Vol. 60, No. 9, 919–920, 1981.
 28. Bruls, R. J., H. T. Hintzen, G. de With, and R. Metselaar, "The temperature dependence of the Young's modulus of MgSiN_2 , AlN and Si_3N_4 ," *Journal of the European Ceramic Society*, Vol. 21, No. 3, 263–268, 2001.
 29. Tomeno, I., "High temperature elastic moduli of Si_3N_4 ceramics," *Japanese Journal of Applied Physics*, Vol. 20, No. 9, 1751–1752, 1981.
 30. Shao, Y., D. Jia, and Y. Zhou, "Effect of porosity on mechanical and dielectric properties of 20% $\text{BN}/\text{Si}_3\text{N}_4$ composite porous ceramics," *Rare Metal Materials and Engineering*, Vol. 38, No. 2, 479–482, 2009.
 31. Liu, H., *Mechanics of Materials*, Higher Education Press, Beijing, China, 2007.